



Anomalous Bloch oscillation and electrical switching of edge magnetization in a bilayer graphene nanoribbon

Tixuan Tan , Fengren Fan, Ci Li ,* and Wang Yao

*Department of Physics, The University of Hong Kong, 999077 Hong Kong, China
and HKU-UCAS Joint Institute of Theoretical and Computational Physics at Hong Kong, 999077 Hong Kong, China*



(Received 16 March 2022; revised 23 June 2022; accepted 27 June 2022; published 6 July 2022)

Graphene features topological edge bands that connect a pair of Dirac points through either sector of the one-dimensional Brillouin zone depending on edge configurations (zigzag or bearded). Because of their flat dispersion, spontaneous edge magnetization can arise from Coulomb interaction in graphene nanoribbons, which has caught a remarkable amount of interest in graphene spintronics. We find an anomalous Bloch oscillation in such edge bands, in which the flat dispersion freezes electron motion along the field direction, while the topological connection of the bands through the bulk leads to electron oscillation in the transverse direction between opposite sides or layers of a bilayer ribbon. Our Hubbard-model mean-field calculation shows that this phenomenon can be exploited for electrical switching of edge magnetization configurations.

DOI: [10.1103/PhysRevB.106.045405](https://doi.org/10.1103/PhysRevB.106.045405)

I. INTRODUCTION

The existence and behavior of edge states are always attractive in the study of solid-state physics due to their distinct properties in contrast to bulk states. Monolayer graphene (MLG) has a zero-gap band structure where the conduction and valance bands touch at the Dirac points [1–6]. Edge states in the MLG ribbon appear as flat bands at the Fermi level, connecting the bulk Dirac points through either sector of the one-dimensional (1D) Brillouin zone depending on edge configurations (zigzag or bearded) [1,2,7–11]. When the bulk gap is opened, these flat-band edge states can be continuously tuned into gapless chiral edge modes through bias control on the edge [7]; these gapless chiral edge modes have a similar origin to that of the topological domain wall modes in bilayer graphene (BLG) [12–14]. In view of their nontrivial topological properties and relation to the bulk valley transport [7,15], these chiral modes have also been explored in other contexts such as the laser-induced Floquet system [16] and gapped nanomechanical graphene [17].

The flat edge band, on the other hand, promises the emergence of magnetism when electron interaction is taken into account [18–21]. In zigzag MLG nanoribbons, the repulsive on-site Coulomb interaction is shown to introduce ground-state spin polarization (SP) on the edges, which can be either antiferromagnetic (AFM) or ferromagnetic (FM), i.e., the localized magnetic moments at the opposite edges of the ribbon are antiparallel or parallel [19–21], turning the system into a semiconductor or a conductor (metal), respectively [18,19]. Based on this phenomenon, some interesting applications in spintronics have been proposed such as half-metallicity induced by an in-plane electric field [19,22] and control of the spin transport by introducing defects [23]. Similar magnetic

effects have also been found in nonstandard-shaped MLG ribbons [24,25].

Compared with MLG ribbons, magnetism in BLG materials and nanostructures is less studied. Most earlier works focused on the half-metallicity and related magnetic effects in zigzag BLG nanoribbons [26–29] or the bulk BLG system [30].

In this paper, we focus on the motions of electrons correlated with the edge states in bearded-zigzag (bea-zig) BLG (the top and bottom layer of a BLG ribbon have zigzag and bearded edges, respectively; the atomic structure and band structure are shown in Fig. 1). The ribbon hosts flat edge bands in the entire 1D Brillouin zone [31]. Under interlayer bias, we find that gapless chiral modes appear in the ribbon bulk near the Dirac point, connecting states localized on opposite edges and layers. Bloch oscillation in the edge bands driven by an electric field along the ribbon has an unusual form in the real space, where the electrons predominantly oscillate in the transverse direction. This brings both edge charge oscillation and layer charge oscillation.

In Sec. II we present and discuss our numerical simulation result for the anomalous Bloch oscillation. Such a phenomenon represents an interesting aspect of Bloch oscillation in real space due to the spatial character of topological edge bands. It is well known that the Chern-number-protected topological edge states also bring Bloch oscillation along the transverse direction [32,33]. However, the phenomena we present in this paper are distinct from those phenomena from several perspectives. (1) The topology involved is different. The anomalous Bloch oscillation presented in this paper is related to a winding number instead of a Chern number, as discussed in our earlier work [31]. In the Chern-number-protected case, the edge states on opposite layers live in the same momentum region, and they belong to different energy bands [32]. They cross each other to connect the bulk bands. In our system, edge states of opposite edges belong to the

*oldsmith@hku.hk

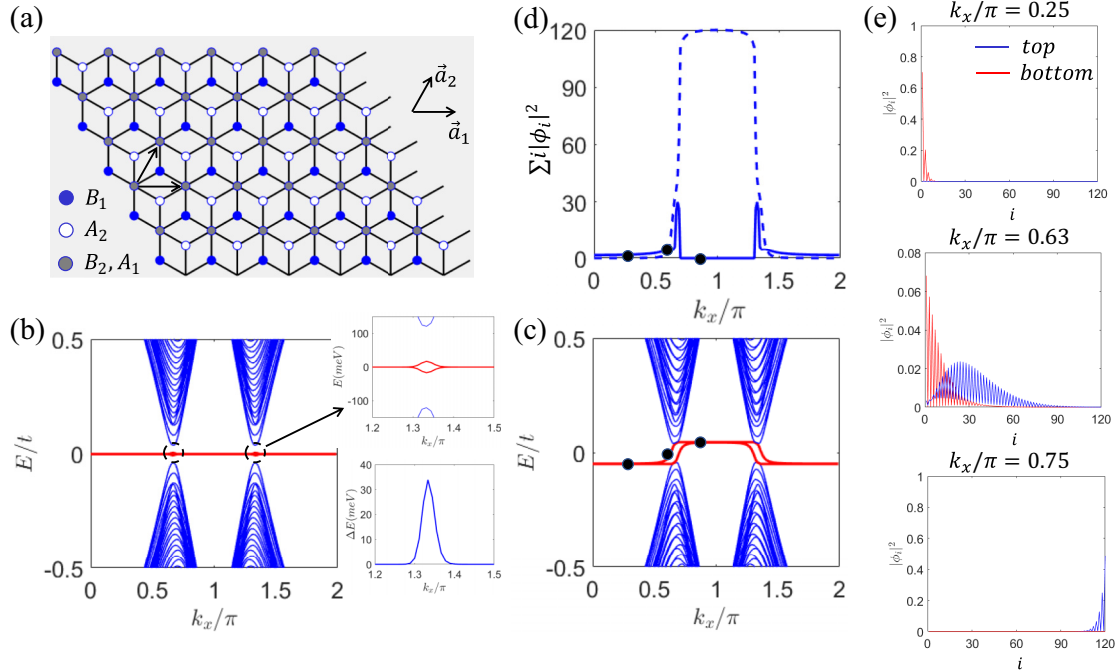


FIG. 1. A schematic illustration of the atomic structure of bea-zig BLG ribbons and related bulk chiral modes. The number of atoms in one unit cell of the ribbon is chosen to be 120 for each layer for all plots. (a) The atomic structure of bea-zig BLG ribbons. The unit vectors are denoted by \vec{a}_1 and \vec{a}_2 . Ribbons are assumed to be infinite along the x , viz., \vec{a}_1 , direction. (b) The band structure for the bea-zig BLG ribbon with no bias. Two edge bands are highlighted by the solid red lines. The zoomed-in band structure in the black dashed circle is shown next to (b), and the energy difference between two edge bands (red solid lines) is presented below. (c) The band structure for the biased bea-zig BLG ribbon. Two bands of edge states are highlighted by the solid red lines. (d) The real space polarization of the wave function, where the wave function is in the form $|\varphi\rangle = \sum \phi_i |i\rangle$ with i labeling sites along the \vec{a}_2 direction. This wave function depicts the higher of the two red bands, with dashed (solid) lines referring to the distribution on the top (bottom) layer. (e) The real space distribution of the wave function of one of the edge states (the higher flat band) with different k_x values, as marked in (c) and (d). The blue (red) solid line refers to the distribution on the top (bottom) layer. The parameters are the interlayer bias $U_1 = 0$ (b) and $U_1 = 0.1t$ (c). $t = 3.16$ eV for all plots.

same band. They live in a different momentum region and are connected with each other near the Dirac points by bulk modes. One consequence of this difference is that the period of oscillation in the momentum space is different: 4π for the Chern-number-protected case and 2π for our case [32]. (2) The winding-number-generated edge bands are flat in most parts of momentum space. The nondispersive nature of the bands makes it possible to freeze the motion along the longitudinal direction, in contrast to the dispersive topological edge states [34]. (3) There is an additional layer degree of freedom in our system compared with the Chern-number-protected case. As will be shown, both edge charge oscillation and layer charge oscillation can be observed in our system.

In Sec. III we include interaction between electrons and discuss possible applications. With Hubbard interaction included through the mean-field approach, we show that the reported anomalous Bloch oscillation can be exploited for electrical switching of the edge magnetization configuration. This points to a possibility of spintronics control. Finally, we give a summary of our findings in Sec. IV.

II. ANOMALOUS BLOCH OSCILLATION

The electronic properties of the biased bea-zig BLG can be described by the tight-binding Hamiltonian [31]

$$H_{\text{BLG}} = H_{\text{bea}}^1 + H_{\text{zig}}^2 + H_{\text{int}} + H_{\text{bias}}, \quad (1)$$

where

$$H_{\text{bea/zig}}^l = -t \sum_{(i,j),\sigma} (c_{l,i,\sigma}^\dagger c_{l,j,\sigma} + \text{H.c.}) \quad (2)$$

represents the tight-binding Hamiltonian of MLG with bearded or zigzag edges and $l = 1, 2$ are labels of the bottom and top layers, respectively. t denotes the nearest-neighbor (NN) hopping in MLG with $c_{i,\sigma}^\dagger$ ($c_{i,\sigma}$) being the creation (annihilation) operator of a σ -spin electron on site i in the ribbon, and $\sum_{(i,j),\sigma}$ only sums over NN pairs. Since there is no Hubbard interaction, i.e., no interaction between different spins, the index σ can be ignored.

$$H_{\text{bias}} = \sum_{l,i,\sigma} (-1)^l \frac{U_1}{2} (c_{l,i,\sigma}^\dagger c_{l,i,\sigma} + \text{H.c.}) \quad (3)$$

refers to the interlayer bias U_1 . The van der Waals interaction between two layers [1,35] is described by H_{int} . In this paper we only consider the NN interlayer coupling γ_1 for simplicity. Here, we take $t = 3.16$ eV and $\gamma_1 = 0.381$ eV as typical experimental values for AB -stacked BLGs [36].

We take the x direction as the infinite direction of the BLG ribbon. For this specific structure, it has been shown in our earlier work [31] that there are two degenerate nondispersive edge bands in the whole k_x region when $U_1 = 0$. They are related with an interlayer-coupling-protected topological

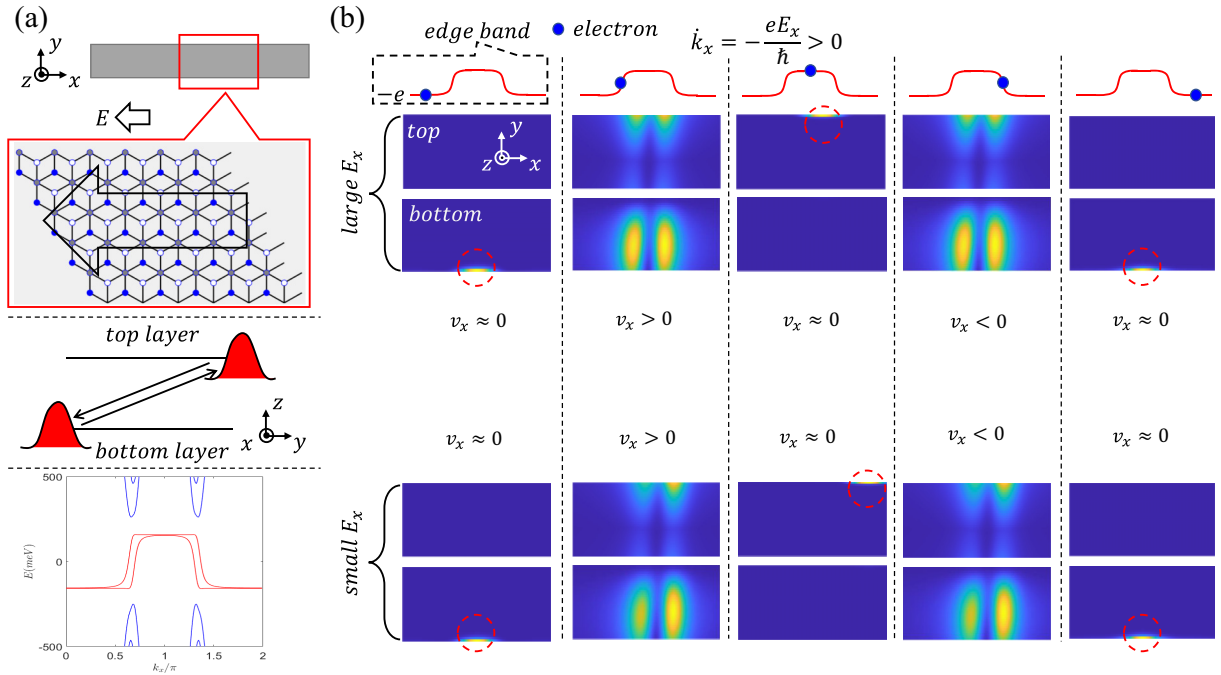


FIG. 2. The numerical simulation of the motion of electrons in real space based on the edge states of the biased bea-zig BLG. The dynamics of electrons is simulated by using Gaussian wave packets in the momentum space, following the procedure outlined in Ref. [37]. (a) Top panel: a schematic illustration of the BLG ribbon on which the simulation is conducted. The x direction is the periodic direction, while y is the finite direction. It is chosen that the length (width) of the ribbon [x (y) direction] is $4800a$, and there are 64 atoms in each layer. a is the lattice constant of graphene. The red box shows the plot range of the simulation, which covers a length of $800a$. Middle panel: schematic illustration of the movement of electrons in the y - z plane perpendicular to the applied external electric field E_x . Bottom panel: band structure of the BLG ribbon used in the simulation. The gap between the red bands and the blue bands (bulk) is around $0.05t$. (b) The result of the numerical simulation when the electron on the edge band moves to different positions in k_x space, as shown in the two rows of panels at top. The color represents the magnitude of the wave function in real space, increasing from blue to yellow. The parameters used are $E_x = -1.7 \times 10^{-2}$ and -2.8×10^{-3} V/nm for the two rows of panels at top and the two rows of panels at bottom, respectively. The color scale is matched within each set of graphs but may vary from set to set. The lower one of the two edge bands is used in the simulation.

phase transition between two nontrivial topological phases characterized by winding number $W = -1$ and $W = 1$ when crossing the Dirac point.

When $U_1 \neq 0$, topological edge states still exist in the whole k_x region with different energy when crossing the Dirac point. They are connected by a pair of bulk chiral modes, as shown in Fig. 1(c). The degeneracy between edges is lifted due to the broken chiral symmetry, as discussed in Ref. [31]. The bulk chiral modes connect states residing on opposite edges of different layers. The connection must be done through the bulk, hence the name.

The fact that these connecting chiral modes are bulk states is by itself interesting in terms of transport. It is often the case that the bulk part of the material is an insulator, so that all electrical transport is dependent on topologically protected edge states. However, in the system we discuss here, transport is done by two special pairs of chiral bulk states, one at each valley. These special bulk states at the Fermi level are present only because there are edge states populating different areas of the momentum space. They are not obtained by discretizing the bulk spectrum of the BLG, e.g., the blue bands in Fig. 1(c).

An interesting application of these bulk chiral modes is Bloch oscillation in the edge bands [32,37–41]. When applying an electric field $eE_x = \frac{\partial A(t)}{\partial t}$ along the infinite direction

(the x direction in our assumption) of the ribbon, the motion of electrons in the edge states can be approximately described by semiclassical equations of a wave packet. The wave vector of the electron will evolve according to $\dot{k}_x = -eE_x/\hbar$, as shown in Fig. 2. Because of the existence of the bulk chiral modes connecting two opposite edges of two different layers, the transition of electrons from the left edge of one layer to the right edge of the other layer is possible, giving rise to a Hall-effect-like behavior of electrons, as illustrated in Fig. 2(a).

The naive conjecture above may be undermined by the smallness of the gap opened by the bias. Numerically, a bias as large as $U_1 = 200$ meV can open a gap of around 5 meV between two edge bands in the flat part. Landau-Zener tunneling may cause the electrons to transit between different edge bands, breaking down our conjecture based upon a single-band picture. However, such a transition is suppressed by the fact that there is no spatial overlap between the wave functions of two flat edge bands, i.e., $\langle \text{edge band 1} | H_{E_x} | \text{edge band 2} \rangle \approx 0$ [42]. The bulk state, i.e., the blue bands as shown in Fig. 1, is also not relevant here since (1) Landau-Zener tunneling between the edge states and bulk states is proved to be highly suppressed [44] and (2) the gap between the bulk bands and the edge bands for the ribbon we use in this simulation is around $0.05t$ for the ribbon used in Fig. 2, which is too large

for the electrical field we use to cause interband transition. Due to these results, we can employ the single-band approximation in our simulation.

Here, we use a wave packet to simulate the motion of electrons in real space. It shows the expected trajectory, as shown in Fig. 2(b). The evolution of the wave packet as demonstrated in Fig. 2 is done by following the procedure of Ref. [37]. The wave packet $|\psi\rangle$ is expanded in the Bloch state basis $|\phi_k\rangle$ of energy $E(k)$ with time-dependent coefficients $c(k, t)$:

$$|\psi(t)\rangle = c(k, t) |\phi_k\rangle, \\ c(k, t) = c(k + Ft/\hbar, 0) \exp\left(\frac{i}{F} \int_{k+ Ft/\hbar}^k E(k') dk'\right), \\ F \equiv eE_x. \quad (4)$$

For the scenario demonstrated in Fig. 2, E_x is negative. The initial wave packet is a Gaussian wave packet centered around the initial momentum $k_0 \approx 0.3\pi$ with the width of the wave packet $\sigma \approx 0.02$:

$$c(k, 0) = \exp\left(-\frac{(k - k_0)^2}{\sigma^2}\right). \quad (5)$$

We note that in the transition between edges, i.e., in the second and the fourth columns of Fig. 2(b), there are two mass centers of the wave packet. This results from our choice of σ . A decrease in σ is observed to eliminate such a feature. Due to this observation, we can attribute the presence of this two-mass-center behavior to the breathing mode of Bloch oscillation [37], i.e., when the wave packet is broad enough in the momentum space, the wave packet will have a constant mean position $\langle x(t) \rangle$ with an oscillating width $\langle \Delta x(t) \rangle$.

It should be noted that the major physics we would like to stress in this section is that the wave packet oscillates in the transverse direction due to the topological property of the bea-zig BLG. This anomalous oscillation is present independent of the choice of σ and k_0 . Results with a narrower width and without two mass centers are demonstrated in the Supplemental Material [45].

In a full cycle, i.e., the momentum k_x evolves from 0 to 2π , a wave packet will move both in the x direction and in the y direction. The motions in these two directions are different. Since only the part of the edge bands near the Dirac points (bulk chiral modes) has nonvanishing group velocity and the time of the wave packet staying in this region is inversely proportional to the field strength, the range of motion of the wave packet in the x direction is inversely proportional to the electric field strength E_x , which can be observed in Fig. 2(b). Also, this range is proportional to the bias as it determines how dispersive the connecting bulk modes are. Thus the motion in the longitudinal direction can be frozen by either using a smaller bias or using a larger field, as shown in the Supplemental Material [45].

However, the range of motion of the anomalous oscillation in the transverse direction, i.e., the y direction, is independent of the field strength, which must be the whole width of the ribbon. Here, we have used $U_1 = 200$ meV in the numerical simulation of Fig. 2. Similar phenomena can still be observed for smaller U_1 or even for $U_1 \approx 0$, where the motion in the x direction is frozen, leaving the oscillation in

the transverse direction unaffected [45]. It should be noted that these phenomena are unique to this bea-zig BLG ribbon, as there are edge bands detached from the bulk bands in the whole Brillouin zone. It is not possible to observe it in the BLG zigzag-zigzag ribbon, as all four of its edge bands only exist in a partial region in momentum space.

III. ELECTRICAL SWITCHING OF EDGE MAGNETIZATION

Magnetic effects of the edge states in the BLG ribbon can be described by self-consistent mean-field calculation when adding the Hubbard interaction H_U to the usual tight-binding Hamiltonian H_{BLG} of the BLG ribbon [18]:

$$H = H_{\text{BLG}} + H_U, \quad H_U = U \sum_i n_{i,\uparrow} n_{i,\downarrow}. \quad (6)$$

The Hubbard interaction H_U represents the electron-electron interaction in the form of the repulsive on-site Coulomb interaction. $n_{i,\uparrow(\downarrow)} \equiv a_{i,\uparrow(\downarrow)}^\dagger a_{i,\uparrow(\downarrow)}$ is the occupation number operator, and $U > 0$ describes its magnitude. We take $U = 1.2t$ in this paper [18].

Since the interaction between different spins is no longer zero, the spin degrees of freedom σ should be considered. We show the band structure of H for both spins in Figs. 3(a) and 4(a). The calculation details and a brief review of the model can be found in the Supplemental Material [45]. Bulk modes connecting edge modes appear that are similar to those arising in the non-Hubbard spinless bea-zig BLG ribbon, as shown in Fig. 3(a). The SP configurations are not limited to two simple types (AFM or FM) as found in the MLG ribbon in Ref. [18]. There are eight inequivalent types of SP for BLG cases, as shown in Table I. For simplicity, in Fig. 3(a) we demonstrate only two types of band structures corresponding to configuration 4 in Table I.

The essence of the result in the spinless model is that an external field E_x can push electrons through the momentum space and cause corresponding motion in the real space. In a spinless model, the occupation of the electrons in the momentum space does not affect the band structure, while the band structure of the Hubbard model is dependent on the momentum space distribution of electrons [18,45]. Thus not all configurations in the momentum space are self-consistent ground states at equilibrium. In fact, as listed in Table I, there are only 16 (8×2) self-consistent solutions of the model. Any unstable configurations should relax into one of them.

An electric field E_x will push the system out of equilibrium by shifting the position of the electrons in momentum space. If the shift is small, it is reasonable to expect that the system should relax to the initial configuration. However, if the shift is large enough in momentum space, the system may relax to another ground state when trying to reach equilibrium. The idea of this procedure is schematically illustrated in Fig. 3(b) [46].

Numerically, this is verified by giving different initial configurations to the electron's momentum space distribution, which would stably converge to a different ground state, as illustrated in Figs. 3(a) and 3(b). Initially, spin-up and spin-down electrons occupy distinct regions in the momentum space. If the electrons are pushed to the positive k_x direction

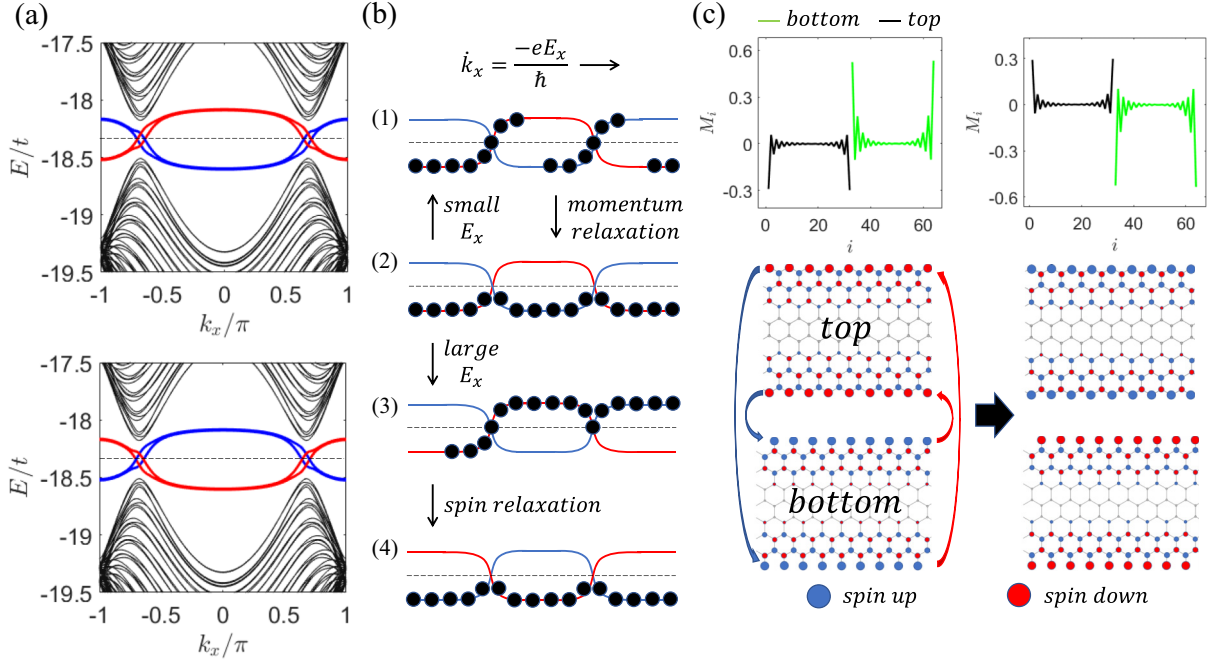


FIG. 3. (a) Band structure of two self-consistent ground states of the bea-zig BLG ribbon in the Hubbard model, corresponding to configuration 4 in Table I. The black dashed line is the Fermi level. Black solid lines are bulk bands. Blue (red) solid lines are edge bands of spin-up (spin-down) electrons. (b) Schematic illustration of the Bloch oscillation in the same system. Condition (2) [(4)] corresponds to the top (bottom) panel of (a). Condition (1) [(3)] is an intermediate state where the deviation from the initial state, i.e., the top panel of (a), is small (large). The black circles are electrons occupying bands. (c) Top panels: SP configurations corresponding to (a) [the left (right) panel corresponds to the top (bottom) panel of (a)], which are defined by the magnetic moment M_i [50]. The black (green) solid line represents the situation on the top (bottom) layer. The horizontal axis is the site index, increasing along the finite direction of the ribbon. The top-layer atoms constitute the first half, while the bottom-layer atoms constitute the second half. Bottom panels: schematic illustration of the SP in real space, corresponding to the SP configurations shown in the top panel. A transition between these two configurations can be induced by the process illustrated in (b).

by a small distance, they will stably converge to the initial state, i.e., the top panel of Fig. 3(a). If electrons are pushed further away from their initial state, they will stably converge to an equilibrium state that differs from their initial state by an exchange of spin, i.e., the bottom panel of Fig. 3(a). The corresponding real space change is illustrated in Fig. 3(c). This is an intraconfiguration transition between ground states, i.e., configuration 4 of Table I. The result in the real space is the exchange of spin polarization between two layers of the ribbon, as shown in Fig. 3(c).

Moreover, we found that the interconfiguration transition between ground states is possible by following a similar process. This is shown in Fig. 4, where configuration 3 in Table I can be transformed into configuration 8 through the exchange of spins between the same edges of different layers. The switch of edge magnetization only happens between two partially filled bands since there are always finite gaps (around 20 meV) between these two bands and the other two bands, i.e., one empty edge band and one fully filled edge band. The gaps are shown in Fig. 4(a).

TABLE I. Summary of self-consistent solutions of bea-zig BLG ribbons. Here, “+” and “-” indicate the sign of the magnetic moment at the corresponding edge; tu (td) represents the up (down) edge of the top layer, while bu and bd are for the edges of the bottom layer (“up” and “down” are relative to the y direction as shown in Fig. 1). SC and C, semiconductor and metal (conductor), respectively. There are altogether 16 configurations; the remaining eight configurations are obtained from these by an exchange between spin-up electrons and spin-down electrons.

Configuration	tu	td	bu	bd	SC or C
1	+	+	+	+	C
2	+	+	+	-	C
3	+	+	-	+	C
4	+	+	-	-	C
5	+	-	+	+	C
6	+	-	+	-	SC
7	+	-	-	+	SC
8	-	+	+	+	C

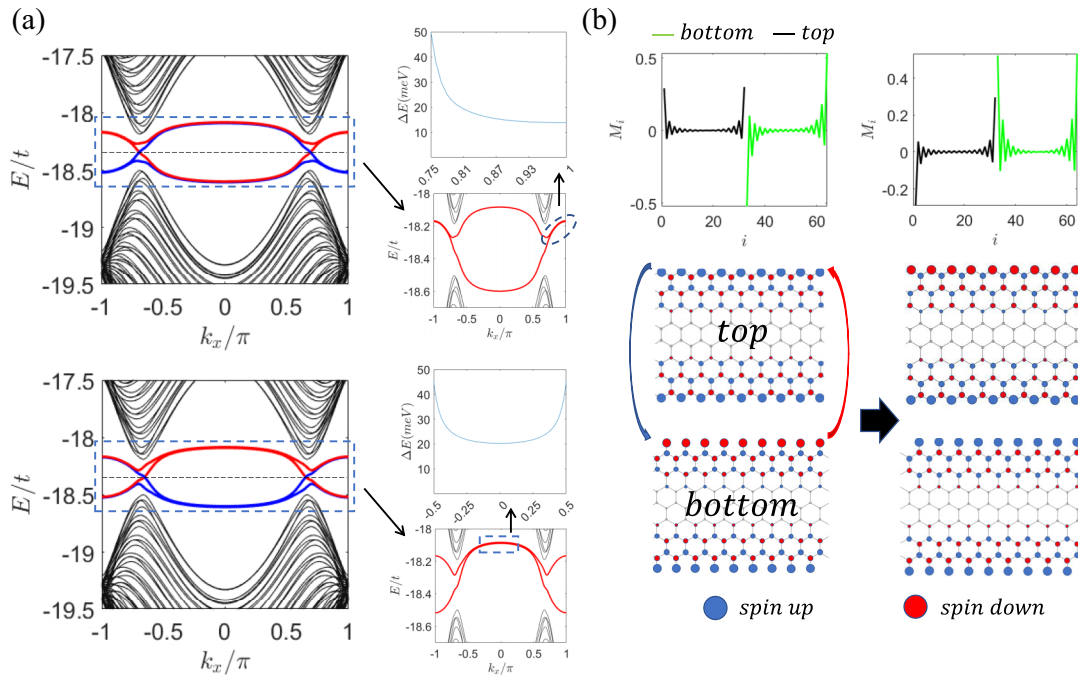


FIG. 4. (a) Band structure of two self-consistent ground states of the bea-zig BLG ribbon in the Hubbard model, corresponding to configurations 3 (top panel) and 8 (bottom panel) in Table I. The black dashed line is the Fermi level. Black solid lines are the bulk bands. Blue (red) solid lines are edge bands of spin-up (spin-down) electrons. The zoomed-in band structures in the blue dashed box are shown next to it, and the related energy difference (around 20 meV) between the nearly degenerate parts is presented above each zoomed-in band structure. (b) Top panels: SP configurations corresponding to (a) [the left (right) panel corresponds to the top (bottom) panel of (a)], which are defined by the magnetic moment M_i [50]. Bottom panels: schematic illustration of the SP distribution in real space, corresponding to the two SP configurations shown in the top panels. A transition between these two SP configurations can be induced based on a process similar to that shown in Fig. 3(b).

IV. CONCLUSIONS AND DISCUSSION

In summary, we study the motions of electrons related to the edge states in bea-zig BLG, with and without Hubbard interaction. The bulk chiral modes connecting two sectors of the Brillouin zone are unconventional. They connect two nontrivial topological phases and are related to the change of topology between sectors.

When applying an electric field along the infinite direction of the ribbon, the motion of electrons in the edge states can be described by Bloch oscillation based on semiclassical equations of wave packets. This leads to layer charge oscillation and edge charge oscillation since the bulk chiral modes connect opposite edges of different layers. Both oscillations are transverse to the field. For the same system with the Hubbard interaction, the Hall-effect-like behavior persists when the electric field is applied, protected by the spatial character of the topological edge bands. Besides, we also exploit the possibility of electrical switching of edge magnetization in the Hubbard model using this bulk mode. With recent progress in the bottom-up approach, synthesizing a long or narrow atomically precise graphene ribbon with well-defined edges has become possible [51–53]. This makes

the testing of edge-induced magnetism in a graphene ribbon, as well as various properties associated with edge topology in a graphene ribbon, possible in the near future. Since all these dynamical effects are related to the bulk chiral states connecting edge states of the system, we can generalize our study to other 2D materials with strong edge effects such as transition metal dichalcogenides [54–56] and materials having kagome [57] or triangular [58,59] lattice structure. All of these are potential directions for further study.

ACKNOWLEDGMENTS

T.T. would like to thank Z. A. Hu and J. W. Li for their generous support in completing this work. C.L. would like to thank D. W. Zhai, B. Fu, and T. Y. Yang for useful discussions. This work was supported by the University Grants Committee/Research Grant Council of the Hong Kong SAR (AoE/P-701/20), Guangdong-Hong Kong Joint Laboratory of Quantum Matter, the HKU Seed Funding for Strategic Interdisciplinary Research, and the Croucher Senior Research Fellowship.

[1] N. M. R. Peres, F. Guinea, and A. H. Castro Neto, Electronic properties of disordered two-dimensional carbon, *Phys. Rev. B* **73**, 125411 (2006); A. H. Castro Neto, F. Guinea,

N. M. R. Peres, K. S. Novoselov, and A. K. Geim, The electronic properties of graphene, *Rev. Mod. Phys.* **81**, 109 (2009).

- [2] V. Meunier, A. G. Souza Filho, E. B. Barros, and M. S. Dresselhaus, Physical properties of low-dimensional sp^2 -based carbon nanostructures, *Rev. Mod. Phys.* **88**, 025005 (2016).
- [3] P. R. Wallace, The band theory of graphite, *Phys. Rev.* **71**, 622 (1947).
- [4] V. P. Gusynin and S. G. Sharapov, Unconventional Integer Quantum Hall Effect in Graphene, *Phys. Rev. Lett.* **95**, 146801 (2005).
- [5] K. S. Novoselov, A. K. Geim, S. V. Morozov, D. Jiang, M. I. Katsnelson, I. V. Grigorieva, S. V. Dubonos, and A. A. Firsov, Two-dimensional gas of massless Dirac fermions in graphene, *Nature (London)* **438**, 197 (2005); M. I. Katsnelson, K. S. Novoselov, and A. K. Geim, Chiral tunnelling and the Klein paradox in graphene, *Nat. Phys.* **2**, 620 (2006); K. S. Novoselov, Z. Jiang, Y. Zhang, S. V. Morozov, H. L. Stormer, U. Zeitler, J. C. Maan, G. S. Boebinger, P. Kim, and A. K. Geim, Room-temperature quantum Hall effect in graphene, *Science* **315**, 1379 (2007).
- [6] Y. B. Zhang, Y.-W. Tan, H. L. Stormer, and P. Kim, Experimental observation of the quantum Hall effect and Berry's phase in graphene, *Nature (London)* **438**, 201 (2005).
- [7] W. Yao, S. A. Yang, and Q. Niu, Edge States in Graphene: From Gapped Flat-Band to Gapless Chiral Modes, *Phys. Rev. Lett.* **102**, 096801 (2009).
- [8] P. Delplace, D. Ullmo, and G. Montambaux, Zak phase and the existence of edge states in graphene, *Phys. Rev. B* **84**, 195452 (2011).
- [9] K. Nakada and M. Fujita, Edge state in graphene ribbons: Nanometer size effect and edge shape dependence, *Phys. Rev. B* **54**, 17954 (1996).
- [10] S. Ryu and Y. Hatsugai, Topological Origin of Zero-Energy Edge States in Particle-Hole Symmetric Systems, *Phys. Rev. Lett.* **89**, 077002 (2002).
- [11] L. Brey and H. A. Fertig, Electronic states of graphene nanoribbons studied with the Dirac equation, *Phys. Rev. B* **73**, 235411 (2006).
- [12] I. Martin, Ya. M. Blanter, and A. F. Morpurgo, Topological Confinement in Bilayer Graphene, *Phys. Rev. Lett.* **100**, 036804 (2008).
- [13] M. Zarenia, J. M. Pereira, Jr., G. A. Farias, and F. M. Peeters, Chiral states in bilayer graphene: Magnetic field dependence and gap opening, *Phys. Rev. B* **84**, 125451 (2011).
- [14] L. Ju, Z. Shi, N. Nair, Y. Lv, C. Jin, J. Velasco, Jr., C. Ojeda-Aristizabal, H. A. Bechtel, M. C. Martin, A. Zettl, J. Analytis, and F. Wang, Topological valley transport at bilayer graphene domain walls, *Nature (London)* **520**, 650 (2015).
- [15] D. Xiao, W. Yao, and Q. Niu, Valley-Contrasting Physics in Graphene: Magnetic Moment and Topological Transport, *Phys. Rev. Lett.* **99**, 236809 (2007); W. Yao, D. Xiao, and Q. Niu, Valley-dependent optoelectronics from inversion symmetry breaking, *Phys. Rev. B* **77**, 235406 (2008).
- [16] P. M. Perez-Piskunow, G. Usaj, C. A. Balseiro, and L. E. F. Foa Torres, Floquet chiral edge states in graphene, *Phys. Rev. B* **89**, 121401(R) (2014).
- [17] X. Xi, J. Ma, S. Wan, C.-H. Dong, and X. Sun, Observation of chiral edge states in gapped nanomechanical graphene, *Sci. Adv.* **7**, eabe1398 (2021).
- [18] O. V. Yazyev, Emergence of magnetism in graphene materials and nanostructures, *Rep. Prog. Phys.* **73**, 056501 (2010).
- [19] Y. W. Son, M. L. Cohen, and S. G. Louie, Half-metallic graphene nanoribbons, *Nature (London)* **444**, 347 (2006).
- [20] F. Muñoz-Rojas, J. Fernández-Rossier, and J. J. Palacios, Giant Magnetoresistance in Ultrasmall Graphene Based Devices, *Phys. Rev. Lett.* **102**, 136810 (2009).
- [21] M. Slota, A. Keerthi, W. K. Myers, E. Tret'yakov, M. Baumgarten, A. Ardavan, H. Sadeghi, C. J. Lambert, A. Narita, K. Müllen, and L. Bogani, Magnetic edge states and coherent manipulation of graphene nanoribbons, *Nature (London)* **557**, 691 (2018).
- [22] S. Dutta, A. K. Manna, and S. K. Pati, Intrinsic Half-Metallicity in Modified Graphene Nanoribbons, *Phys. Rev. Lett.* **102**, 096601 (2009).
- [23] M. Wimmer, Í. Adagideli, S. Berber, D. Tománek, and K. Richter, Spin Currents in Rough Graphene Nanoribbons: Universal Fluctuations and Spin Injection, *Phys. Rev. Lett.* **100**, 177207 (2008).
- [24] Z. F. Wang, S. Jin, and F. Liu, Spatially Separated Spin Carriers in Spin-Semiconducting Graphene Nanoribbons, *Phys. Rev. Lett.* **111**, 096803 (2013).
- [25] X. X. Li and J. L. Yang, First-principles design of spintronic materials, *Nat. Sci. Rev.* **3**, 365 (2016).
- [26] B. Sahu, H. K. Min, A. H. MacDonald, and S. K. Banerjee, Energy gaps, magnetism, and electric-field effects in bilayer graphene nanoribbons, *Phys. Rev. B* **78**, 045404 (2008).
- [27] V. N. Kotov, B. Uchoa, V. M. Pereira, F. Guinea, and A. H. Castro Neto, Electron-electron interactions in graphene: Current status and perspectives, *Rev. Mod. Phys.* **84**, 1067 (2012).
- [28] G. W. Jeon, K. W. Lee, and C. E. Lee, Layer-selective half-metallicity in bilayer graphene nanoribbons, *Sci. Rep.* **5**, 9825 (2015); K. W. Lee and C. E. Lee, Half-metallic quantum valley Hall effect in biased zigzag-edge bilayer graphene nanoribbons, *Phys. Rev. B* **95**, 085145 (2017); Topological confinement effects of electron-electron interactions in biased zigzag-edge bilayer graphene nanoribbons, **97**, 115106 (2018).
- [29] K. Szałowski, Ferrimagnetic and antiferromagnetic phase in bilayer graphene nanoflake controlled with external electric fields, *Carbon* **118**, 78 (2017).
- [30] J. Yuan, D.-H. Xu, H. Wang, Y. Zhou, J.-H. Gao, and F.-C. Zhang, Possible half-metallic phase in bilayer graphene: Calculations based on mean-field theory applied to a two-layer Hubbard model, *Phys. Rev. B* **88**, 201109(R) (2013).
- [31] T. Tan, C. Li, and W. Yao, Edge state in AB-stacked bilayer graphene and its correspondence with the Su-Schrieffer-Heeger ladder, *Phys. Rev. B* **104**, 245419 (2021).
- [32] C. Li, W. Zhang, Y. V. Kartashov, D. V. Skryabin, and F. Ye, Bloch oscillations of topological edge modes, *Phys. Rev. A* **99**, 053814 (2019).
- [33] Z. G. Chen, W. Y. Tang, R. Y. Zhang, Z. X. Chen, and G. C. Ma, Landau-Zener Transition in the Dynamic Transfer of Acoustic Topological States, *Phys. Rev. Lett.* **126**, 054301 (2021).
- [34] The only dispersive region, i.e., the region where the electrons have nonvanishing velocity, are the connecting bulk modes, corresponding to the second and the fourth columns of Fig. 2(b). As discussed later, this region is tunable by applying a different bias, where the smaller bias tends to make the region less dispersive. In the limit of zero bias, the motions of electrons along the longitudinal direction will be frozen.

- [35] E. McCann and V. I. Fal'ko, Landau-Level Degeneracy and Quantum Hall Effect in a Graphite Bilayer, *Phys. Rev. Lett.* **96**, 086805 (2006); E. McCann and M. Koshino, The electronic properties of bilayer graphene, *Rep. Prog. Phys.* **76**, 056503 (2013).
- [36] A. B. Kuzmenko, I. Crassee, D. van der Marel, P. Blake, and K. S. Novoselov, Determination of the gate-tunable band gap and tight-binding parameters in bilayer graphene using infrared spectroscopy, *Phys. Rev. B* **80**, 165406 (2009).
- [37] T. Hartmann, F. Keck, H. J. Korsch, and S. Mossmann, Dynamics of Bloch oscillations, *New J. Phys.* **6**, 2 (2004).
- [38] V. Krueckl and K. Richter, Bloch-Zener oscillations in graphene and topological insulators, *Phys. Rev. B* **85**, 115433 (2012).
- [39] X.-J. Liu, K. T. Law, T. K. Ng, and P. A. Lee, Detecting Topological Phases in Cold Atoms, *Phys. Rev. Lett.* **111**, 120402 (2013).
- [40] M. Atala, M. Aidelsburger, J. T. Barreiro, D. Abanin, T. Kitagawa, E. Demler, and I. Bloch, Direct measurement of the Zak phase in topological Bloch bands, *Nat. Phys.* **9**, 795 (2013).
- [41] M. Di Liberto, N. Goldman, and G. Palumbo, Non-Abelian Bloch oscillations in higher-order topological insulators, *Nat. Commun.* **11**, 5942 (2020).
- [42] One can also understand this fact from the well-known formula describing Landau-Zener tunneling [43]: $P = e^{-2\pi\Delta^2\tau}$. Here, P is the transition probability between two bands, Δ is approximately the gap between two bands, and $\frac{1}{\tau}$ is approximately the asymptotic slope of the band. Since τ is infinitely large for our topological flat edge bands and Δ is finitely small, the transition is infinitely suppressed. When near the Dirac point, two edge bands become dispersive, and their wave functions have appreciable overlap. However, a gap around 30 meV is opened even for a zero-bias situation, as shown in Fig. 1, which makes the interband transition near the Dirac point still weak. Combined with the arguments in the main text, this makes the single-band approximation a reasonable assumption.
- [43] A. Dutta, G. Aeppli, B. K. Chakrabarti, U. Divakaran, T. F. Rosenbaum, and D. Sen, *Quantum Phase Transitions in Transverse Field Spin Models: From Statistical Physics to Quantum Information* (Cambridge University Press, Delhi, 2015).
- [44] G. J. Ferreira, R. P. Maciel, P. H. Penteado, and J. C. Egues, Zitterbewegung and bulk-edge Landau-Zener tunneling in topological insulators, *Phys. Rev. B* **98**, 165120 (2018).
- [45] See Supplemental Material at <http://link.aps.org/supplemental/10.1103/PhysRevB.106.045405> for Bloch oscillation behavior with smaller bias and details regarding the self-consistent mean-field calculation.
- [46] The difference between the small and large deviation is the magnitude of the electric field. Here, the important time scales are the momentum relaxation time τ_p and the spin relaxation time τ_s . In graphene, the typical τ_p is of the order of 1 ps [47], and τ_s can be of the order of ~ 10 – 100 ps [48,49]. If the field is too small and relaxation sets in before the deviation is large enough, this corresponds to condition (1) of Fig. 3(b). In contrast, if the field is large enough to take electrons far away from the initial configuration in the momentum space within τ_p , then this corresponds to condition (3) of Fig. 3(b), which makes the switch of ground state possible under the spin relaxation. Therefore it is easy to give an estimated threshold electric field for the switching described in this paper: $E_{\text{threshold}} \sim \frac{\pi\hbar}{ae\tau_p} \sim 10^{-2}$ V/nm, where $a = 0.246$ nm is the lattice constant of MLG.
- [47] C. Ertler, S. Konschuh, M. Gmitra, and J. Fabian, Electron spin relaxation in graphene: The role of the substrate, *Phys. Rev. B* **80**, 041405(R) (2009).
- [48] V. K. Dugaev and M. I. Katsnelson, Spin relaxation related to edge scattering in graphene, *Phys. Rev. B* **90**, 035408 (2014).
- [49] M. I. Katsnelson, *The Physics of Graphene*, 2nd ed. (Cambridge University Press, Cambridge, 2020).
- [50] The SP is expressed by the magnetic moment $M_i \equiv \langle n_{i,\uparrow} \rangle - \langle n_{i,\downarrow} \rangle$ at site i , and the average spin-up or spin-down electron population, $\langle n_{i,\uparrow} \rangle$ or $\langle n_{i,\downarrow} \rangle$, is determined by the self-consistent mean-field calculation (see Ref. [45] for details). In this paper, we take $t = 3.16$ eV [36].
- [51] J. Pijeat, J.-S. Lauret, and S. Campidelli, Bottom-up approach for the synthesis of graphene nanoribbons, in *Graphene Nanoribbons*, edited by L. Brey, P. Seneor, and A. Tejeda (Institute of Physics, Bristol, 2020), Chap. 2, pp. 2-1–2-25.
- [52] C. Backes, A. M. Abdelkader, C. Alonso, A. Andrieux-Ledier, R. Arena, J. Azpeitia, N. Balakrishnan, L. Banszerus, J. Barjon, R. Bartali, S. Bellani, C. Berger, R. Berger, M. M. Bernal Ortega, C. Bernard, P. H. Beton, A. Beyer, A. Bianco, P. Bøggild, F. Bonaccorso *et al.*, Production and processing of graphene and related materials, *2D Mater.* **7**, 022001 (2020).
- [53] P. Ruffieux, S. Wang, B. Yang, C. Sánchez-Sánchez, J. Liu, T. Dienel, L. Talirz, P. Shinde, C. A. Pignedoli, D. Passerone, T. Dumslaff, X. Feng, K. Müllen, and R. Fasel, On-surface synthesis of graphene nanoribbons with zigzag edge topology, *Nature (London)* **531**, 489 (2016).
- [54] D. Wu, X. Li, L. Luan, X. Wu, W. Li, M. N. Yogeesh, R. Ghosh, Z. Chu, D. Akinwande, Q. Niu, and K. Lai, Uncovering edge states and electrical inhomogeneity in MoS₂ field-effect transistors, *Proc. Natl. Acad. Sci. USA* **113**, 8583 (2016).
- [55] C. Zhang, Y. Chen, J.-K. Huang, X. Wu, L.-J. Li, W. Yao, J. Tersoff, and C.-K. Shih, Visualizing band offsets and edge states in bilayer-monolayer transition metal dichalcogenides lateral heterojunction, *Nat. Commun.* **7**, 10349 (2016).
- [56] G. Yang, Y. Shao, J. Niu, X. Ma, C. Lu, W. Wei, X. Chuai, J. Wang, J. Cao, H. Huang, G. Xu, X. Shi, Z. Ji, N. Lu, D. Geng, J. Qi, Y. Cao, Z. Liu, L. Liu, Y. Huang *et al.*, Possible Luttinger liquid behavior of edge transport in monolayer transition metal dichalcogenide crystals, *Nat. Commun.* **11**, 659 (2020).
- [57] H. R. Xue, Y. H. Yang, F. Gao, Y. D. Chong, and B. L. Zhang, Acoustic higher-order topological insulator on a kagome lattice, *Nature Mater.* **18**, 108 (2019).
- [58] P. Nataf, M. Lajkó, A. Wietek, K. Penc, F. Mila, and A. M. Läuchli, Chiral Spin Liquids in Triangular-Lattice SU(N) Fermionic Mott Insulators with Artificial Gauge Fields, *Phys. Rev. Lett.* **117**, 167202 (2016).
- [59] T. Kurumaji, T. Nakajima, M. Hirschberger, A. Kikkawa, Y. Yamasaki, H. Sagayama, H. Nakao, Y. Taguchi, T.-H. Arima, and Y. Tokura, Skyrmion lattice with a giant topological Hall effect in a frustrated triangular-lattice magnet, *Science* **365**, 914 (2019).